Journal of Power Sources 196 (2011) 4324–4331

Contents lists available at ScienceDirect

Journal of Power Sources

journal homepage: www.elsevier.com/locate/jpowsour

Effect of cobalt incorporation in copper-ceria based anodes for hydrocarbon utilisation in Intermediate Temperature Solid Oxide Fuel Cells

A. Fuerte[a,*], R.X. Valenzuela[a], M.J. Escudero[a], L. Daza[a,b]

[a] CIEMAT, Departamento de Energía, Av. Complutense 22, 28040 Madrid, Spain
[b] Instituto de Catálisis y Petroleoquímica (CSIC), Marie Curie 2, Campus Cantoblanco, 28049 Madrid, Spain

ARTICLE INFO

Article history:
Received 30 July 2010
Received in revised form
22 November 2010
Accepted 15 December 2010
Available online 24 December 2010

Keywords:
SOFC anodes
(Co,Cu)-ceria
Single-cell performance
Methane

ABSTRACT

MCuCo40 (CuCo-CeO_2, 40 at.% metal load, 1/1 Cu–Co atomic ratio), synthesised by inverse microemulsion method, was evaluated as the anode for SOFC at intermediate temperature. This material presents optimal physicochemical and electrical characteristics as well as excellent thermal and chemical compatibility with 8YSZ electrolyte. The evaluation of single-cell performance, with 8YSZ electrolyte and LSM cathode and this anode material, operating in H_2 and methane fuels, in comparison with a similar single-cell using Cu-ceria-based anode allows to conclude that the substitution of copper (20 at.%) by cobalt in the anode composition enhances the single cell performance as well as reduces the carbon deposit formation on the anode after running on hydrocarbon fuels (methane).

1. Introduction

Direct utilisation of hydrocarbons in fuel cell systems, without first reforming those fuels to syngas, could provide significant advantages [1]. Theoretically, direct utilisation is possible in solid oxide fuel cells (SOFCs) but it is usually not possible in the absence of added steam because Ni, the most commonly used material in SOFC anodes, catalyses the formation of carbon deposits [2].

Different strategies have been proposed to avoid the deactivation for carbon deposition, for instance by replacing Ni with electronic conductors that no catalyse carbon formation, such as copper [3] or conducting oxides [4]. Unfortunately, it is difficult to achieve sufficient conductivity with oxides under reducing conditions of the anode. Cu-ceria based anodes have allowed to achieve reasonable power densities working on hydrocarbons however, they are limited to relative low operation temperatures (<800 °C), because their tendency to sinter together with the low catalytic activity of copper for C–H scission [5]. A possible solution to these problems involves the use of anodes based on metal alloys or bimetallic systems [6]. The evaluation of Cu–Ni alloys demonstrated that carbon formation was strongly suppressed compared to nickel anodes [7] but their stability were limited in the presence of hydrocarbon.

Ni and Co have similar catalytic properties for hydrocarbon reactions; but the Cu–Ni and Cu–Co systems provide an interesting contrast in that Cu and Ni are completely miscible while Cu and Co are not, being of great interest for SOFC anode development [8].

In a previous work [9], a Cu-doped ceria anode (MCu40, 40 at.% Cu) was evaluated as anode of a single cell, with 8YSZ electrolyte. This anode material showed the ability to operate with methane (80:20 CH_4/H_2) at relative low temperature (750 °C). Unfortunately, the formation of carbon deposits entailed a continuous and rapid lost of cell performance running in pure methane. In this context, the present work is focused on preparation and single cell evaluation of bimetallic Cu–Co-ceria, named hereafter MCuCo40. The comparative study of both materials bimetallic Cu–Co (MCuCo40) and monometallic (MCu40) will allow us to evaluate the effect of the partial substitution (20 at.%) of copper for cobalt in the anode composition on the final cell performance running with hydrogen and/or methane as fuels.

2. Experimental

2.1. Synthesis and characterisation of anode material

Materials combining Cu and Cu–Co with CeO_2 (MCu40 and MCuCo40, respectively), with total metal loading of 40 wt.% (1/1 atomic ratio for bimetallic Cu–Co system), were prepared by coprecipitation within reverse microemulsions; details of the method can be found elsewhere [10]. The resulting material is then calcined under air at 750 °C during 2 h, employing relatively slow heating

* Corresponding author. Tel.: +34 913460897; fax: +34 913466269.
E-mail address: araceli.fuerte@ciemat.es (A. Fuerte).

0378-7753/$ – see front matter © 2010 Elsevier B.V. All rights reserved.
doi:10.1016/j.jpowsour.2010.12.053

ramp of 1 °C min^{-1}. The physicochemical as well as electrochemical characterisation as anode in a single cell of the reference material MCu40 has been previously reported [9].

XRD patterns was recorded at room temperature using a step scan procedure (0.04°/2θ step, time per step 2 s) in the 2θ range 20–80° on a Seifert diffractometer equipped with a crystal monochromator employing Cu Kα radiation (λ = 1.5418 Å).

Chemical compatibility tests were carried out to assess the interaction between anode and electrolyte (8YSZ, Pi-Kem) materials. Equal amount of MCuCo40 and electrolyte were thoroughly ground in an agate mortar and put into a quartz reactor. The mixture was fired in pure hydrogen for 50 h at 750 °C. After completion, XRD partners were recorded following the same conditions described above.

Thermal expansion coefficients (TEC) were measured on an alumina dilatometer Linseis L75/1550, from room temperature to 750 °C, with a heating rate of 5 °C min^{-1} and a 2 h dwell time at maximum temperature, under air and reducing atmosphere (10% H_2/N_2). Previous to these measurements, sample was cold pressed into pellets and then calcined for 2 h to 750 °C.

Electrical conductivity was measured under reducing atmosphere (10% H_2/N_2) as a function of temperature (500–750 °C) by the conventional DC four-terminal method with a multimeter (Agilent 34401A) and a dual output DC power supply (Solartron 1286). For this purpose sample was cold pressed (2 ton cm^{-2}) into rectangular bars (20 mm × 6 mm × 2 mm) and sintered in air at 750 °C for 2 h. Gold paste was used in order to facilitate good electrical contact.

Catalytic activity measurements for oxidation of methane were performed in a tubular quartz reactor operating at atmospheric pressure using 0.5 g of catalysts (0.25–0.42 mesh) packed on a bed of quartz wool and employing 20 ml min^{-1} of 5% H_2/Ar. Heating ramps of 2 °C min^{-1} up to 750 °C, maintaining finally this temperature for 2 h under the reactant mixture, were used. Meanwhile, this activation process has to match the working conditions under which the material works in the electrochemical cell. After reduction, the samples were cooled down to 400 °C and a reactant mixture of CH_4 and O_2 was introduced into the reactor with an inert (Ar) to maintain a constant reactor flow rate. The activity was monitored at temperatures from 400 °C to 750 °C. The react composition included 25% CH_4 and 5% O_2 balance with Ar. Reactants and products were analysed on-line by a gas chromatograph equipped with a TCD. TPO experiments were carried out using a Mettler Toledo TGA/SDTA 851e thermo-balance by introducing 10% O_2 in Ar with a flow rate of 25 ml min^{-1}. The temperature was increased from room temperature to 1000 °C at rate of 10 °C min^{-1}.

2.2. Single cell fabrication and test

The single cell was 1.1 cm diameter and contained a dense 8YSZ electrolyte layer (0.23 μm thick) attached to a porous 8YSZ layer (≈100 μm thick), prepared by tape casting method using PMMA as pore former and then annealing in air at 1400 °C for 2 h. A lanthanum strontium manganite (LSM, NextEnergy) layer was deposited onto the exposed surface of dense electrolyte to form the cathode. The anode catalyst ink was prepared by mixing MCuCo40 powders and the desired amount of binder (Decoflux-DW41), applied onto the YSZ porous layer by screen-printing method and then calcined at 750 °C. Platinum and gold, pastes and wires, were used as current collector for cathode and anode respectively. Finally, cell was attached to an alumina tube with a ceramic seal (Aremco, Ceramabond 552) and placed into a furnace. The single cell active area was 0.38 cm^2.

For comparison, a single cell with the same active area, electrolyte (0.25 mm thick) and cathode but using reference material MCu40 as anode (Cu-CeO_2, 40 at.% Cu) was also fabricated in the same way. Results of this single cell evaluation as well as additional details of preparation method have been reported in our previous work [9].

Humidified hydrogen and or methane were supplied to the anode as fuel at a flow rate of 50 ml min^{-1} after passing through a saturator at room temperature to adjust the gas humidity at 3% H_2O. Cathode was open to air. Long periods of time were used for methane cell exposures (1–4 h) and at least 1 h for recovering in order to reach a steady power output.

For start-up and cell stabilisation, operating temperature (750 °C) was achieved at the rate of 1 °C min^{-1} under humidified hydrogen. Anode was reduced in situ for 24 h. For stabilisation, cell was operating in galvanostatic mode at the selected operating temperature and gas conditions for at least 24 h at a current density of 105 mA cm^{-2}.

Cell performance was evaluated under galvanostatic control at the relative low operating temperature of 750 °C. Voltage as function of time and fuel composition, at constant current density, was measured for evaluating the endurance of the single cell. Electrochemical characterisation including current–voltage (*I–V*) curves, current–power (*I–P*) curves, runtime–power curve (*t–P*) and impedance measurements were conducted using an Autolab system (PGSTAT30 and FRA2 module, Eco Chemie). The impedance of the cell was recorded at open circuit in galvanostatic mode over the frequency range from 1 MHz to 0.01 Hz and excitation signal of 5 mA.

Microstructure and morphology of the single cell and its components after operation were analysed by a scanning electron microscopy (SEM, Hitachi S-2500), equipped with an X-ray analyzer for energy dispersive X-ray spectroscopy (EDX).

3. Results and discussion

3.1. Anode material characterisation

MCuCo40 was prepared by coprecipitation within reverse microemulsion with a total metal loading of 40 at.% (1/1 Cu–Co atomic ratio). As reference material, the basic configuration copper-ceria (MCu40, Cu-CeO_2, 40 at.% Cu) was prepared following the same method. The XRD pattern for MCuCo40 in its initial calcined state reveals that sample is mainly constitutes by the fluorite phase of the mixed oxide $Cu_xCo_yCe_{1-x-y}O_{2-\delta}$ and additional crystalline phases of metallic oxides CuO and Co_3O_4 (Fig. 1). Note that for the monometallic reference material MCu40 [9], fluorite phase of the mixed oxide $Cu_xCe_{1-x}O_{2-\delta}$ coexists with that for metal oxide in its highest oxidation state (CuO, tenorite). For cobalt, it is well known that there are two stable oxides CoO and Co_3O_4 but CoO is thermodynamically stable at temperatures of 900 °C, whereas Co_3O_4 is formed at lower temperatures [11].

In a previous work of our group [10], it was demonstrated that doping of ceria with Cu induces changes in the lattice parameter. Taking into account the ionic radius of Cu^{2+} (0.73 Å) and that of Ce^{4+} (0.97 Å) a large decrease in the lattice parameter should be expected with the increase in Cu^{2+} ions substitution in the fluorite structure. But, simultaneously an increase in the oxygen vacancy is promoted for the substitution of Ce^{4+} with Cu^{2+} ions, therefore, a moderate decrease in the lattice parameter *a* is observed. In the case of bimetallic sample MCuCo40 (*a* = 5.433 Å), in comparison with monometallic MCu40 (*a* = 5.422 Å), the substitution of 20 at.% Cu for cobalt in the anode composition induces a discrete increase in the lattice parameter consistent with the slightly higher ionic radii and the same charge of these two ions (Cu^{2+} = 0.73 Å, Co^{2+} = 0.74 Å).

Under working anode conditions, high temperature and reducing atmosphere, full reduction of metal oxides to the corresponding

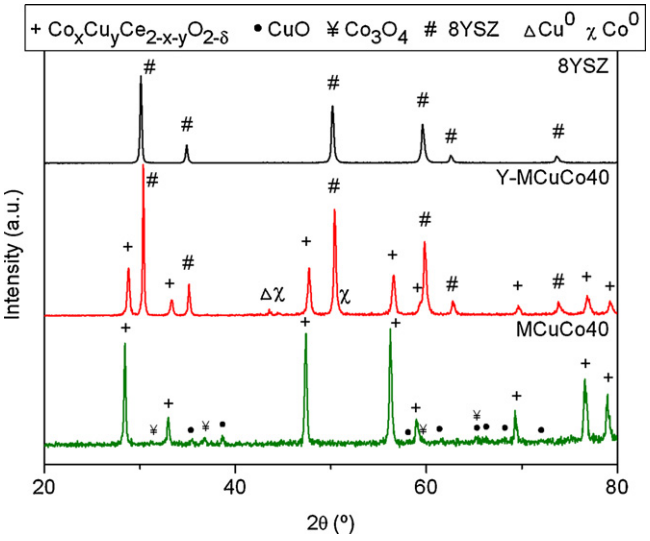

Fig. 1. XRD patterns for 8YSZ, MCuCo40 in its initial calcined state and chemical compatibility test between MCuCo40 and 8YSZ (Y-MCuCo40).

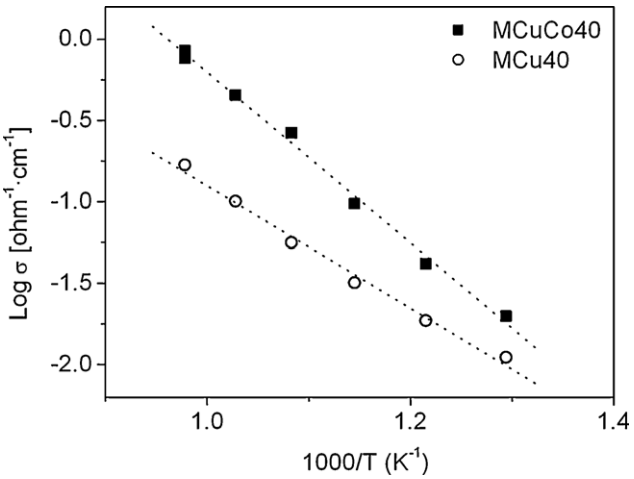

Fig. 2. Electrical conductivity for MCuCo40 (square) and reference material MCu40 (circle) as function of temperature.

metallic states is detected; Cu^0, together with Co^0 for bimetallic sample, coexists with the mixed oxide in both materials MCuCo40 and MCu40.

One characteristic that determines the validity for using an anode material in SOFC is the chemical compatibility between electrode and electrolyte; it is a prerequisite to any further cell testing. Indeed, the formation of reaction products at the electrode/electrolyte interface could be detrimental to the cell efficiency. The cationic inter-diffusion has to be limited in order to prevent the degradation of electrode and electrolyte materials properties. In this sense, reactivity studies were carried out to assess the interaction between the anodic formulation MCuCo40 and 8YSZ electrolyte. XRD pattern for the electrode–electrolyte mixture after lengthy reducing treatment (Y-MCuCo40) is presented for their comparison in Fig. 1, together with pattern for MCuCo40 in its initial calcined state and 8YSZ electrolyte. Results clearly allow to dismiss any chemical reaction between electrode and electrolyte materials, no new phases or changes are observed, only diffraction peaks for both cubic phases of cerium-doped oxide ($Cu_xCo_yCe_{1-x-y}O_{2-\delta}$) and yttria stabilised zirconia (8YSZ). The unique noticeable change was the total reduction of copper and cobalt oxides present on the surface before beginning this treatment, which separately coexist without alloy formation.

As important as a good electrode–electrolyte thermal compatibility the thermal expansion coefficient (TEC), this must be similar to the electrolyte in order to prevent the cell degradation in the heat–cool processes. MCuCo40 has shown a lineal thermal expansion behaviour in air, from 200 °C to 750 °C, with a calculated value for TEC of $9.5 \times 10^{-6}\,K^{-1}$. However, it became steeper under reducing atmosphere (10% H_2/N_2), the slope of the thermal expansion curve increased significantly at about 550 °C as a result of the loss of lattice oxygen and the formation of oxygen vacancies under measuring conditions [12]. TEC value calculated from 200 °C to 550 °C under hydrogen was $12.3 \times 10^{-6}\,K^{-1}$. A similar behaviour was observed with MCu40 sample [9]; TEC values for both samples are in good agreement with those for SOFC electrolytes and thus, it can be concluded that they present a good thermal compatibility with the 8YSZ electrolyte.

The electrical conductivity of sintered samples was measured as function of temperature (500–750 °C) in the presence of 10% H_2/N_2, by the conventional DC four-probe method. Fig. 2 shows the corresponding Arrhenius plots for the samples that have been studied. The relationships in this figure were approximately linear, and no breakpoint exists. Electrical conductivity slightly increases with the cobalt presence from 0.61 S cm^{-1} to 0.85 S cm^{-1} for MCu40 and MCuCo40 at 750 °C and $pO_2 = 10^{-23}$ atm, respectively. It should be due to the extrinsic defects created by substitution of metal ions for cerium ions in CeO_2. The slopes of the lines, that represent the activation energies for the total conductivity, presents differences (0.78 eV and 1.04 eV for both samples, respectively) and suggest that the mechanism of conduction is altered by the ion cobalt into the fluorite structure of CeO_2, due probably a transition from conductivity regimes. With the aim of elucidating the electrical conduction mechanism experiments as function of the oxygen partial pressure are ongoing.

3.2. Catalytic activity measurements

In order to assess the chemical processes taking place at the anode surface of both single cells, the catalytic properties of MCuCo40 and MCu40 samples for direct oxidation of methane has been evaluated. Blank test carried out in the blank reactor, filled only by SiC to avoid hot spots, under the same experimental conditions, showed that conversion was less than 0.1% in all cases.

The results of testing of materials MCuCo40 and MCu40 reference material are given in Fig. 3. Hydrogen selectivity in percent was calculated based in the relation of moles of hydrogen and water produced $[(nH_2/(nH_2 + nH_2O)) \times 100]$. A process of methane oxidation on both samples took place similarity depending on temperature. Firstly, the reaction started at 500 °C, where methane did not react with oxygen at all, and showed that a fairly low hydrogen concentration started at 650 °C. Both samples exhibited similar activity at low temperature, while the conversion increase around 10% with the presence of cobalt in the sample composition at high temperature; however differences in the selectivity to H_2 was quite similar, only a small difference was observed, reached around 40% at 750 °C, although the conversion did not overcame 10% in any case.

Behind cooling the reactor in inert flow and post analysis test, MCu40 showed carbon deposition neighbourhood of the catalytic bed, suggested that methane conversion proceeds also via combustion, however the catalyst of MCuCo40 displayed, at a glance, few carbon build-up was observed. It should be noted that, in order to determine whether the observed deactivation is due to the carbon formation, the post-reaction temperature programmed oxidation (TPO) experiments were carried out.

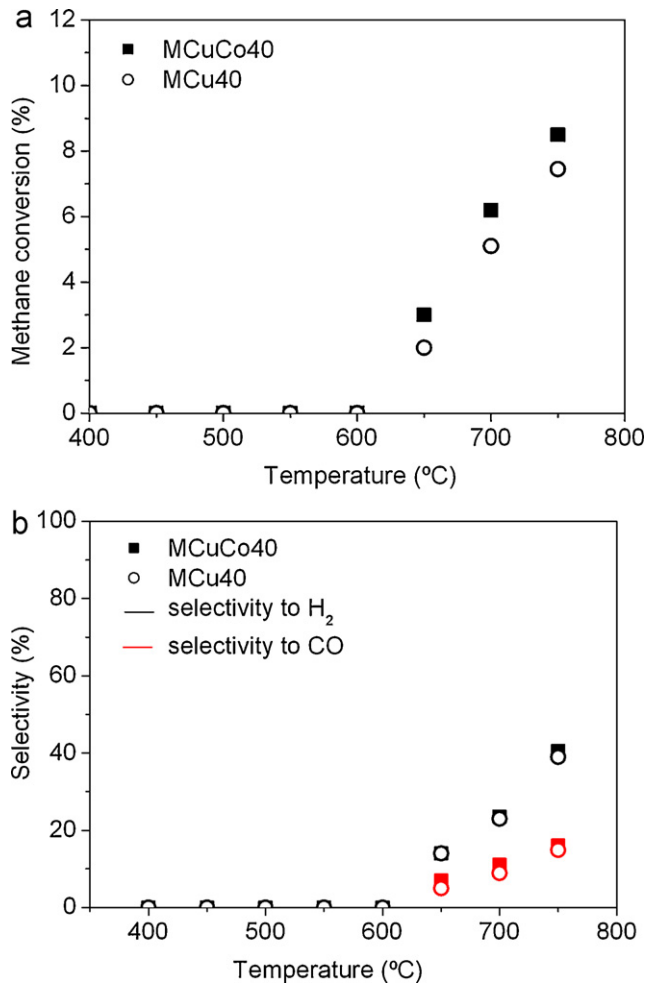

Fig. 3. CH_4 conversion and H_2 and CO selectivity as a function of temperature.

Fig. 4, corresponding to MCu40 TPO results, shows clearly different four peaks of CO_2 (m/z = 44) formed a shoulder at 450 °C and a similar double-peak at 550 °C and 600 °C, related to different carbon species. Some authors attributed the high-temperature peaks (higher than 600 °C) to refractory or inert coke, whereas a more reactive coke (lower than 600 °C) is probably associated with amorphous carbonaceous deposits. The shift of the CO_2 peak to the higher temperature, (~650 °C) was regarded to be inactive and thus responsible for the deactivation, also indicates the increasing difficulty in eliminating such deposited carbon, while the carbonaceous species, do not have a negative effect, and would be considered

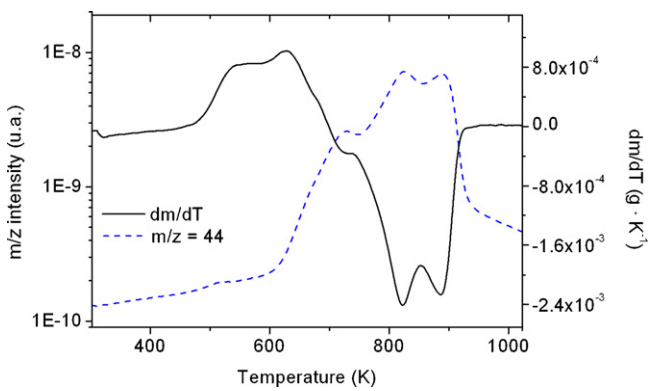

Fig. 4. TPO results for MCu40 sample.

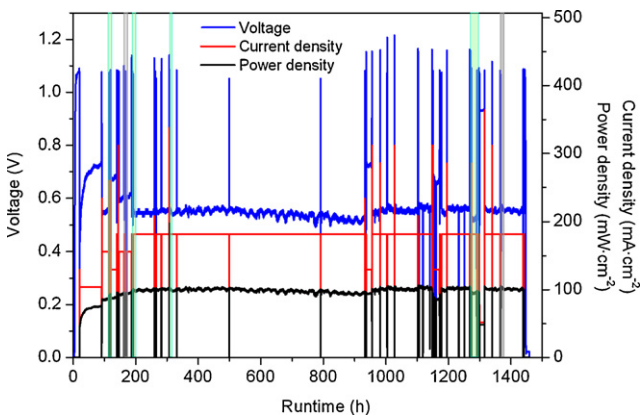

Fig. 5. Global cell performance of MCuCo40/8YSZ/LSM single cell as function of current density and fuel composition. Methane exposure: 80:20 CH_4/H_2 (solid green bars); 100% CH_4 (solid grey bars). (For interpretation of the references to color in this figure legend, the reader is referred to the web version of the article.)

reversibly converted to CO by CO_2 oxidation [13]. The TPO analysis of MCuCo40 gave evidences of lower level formation of carbonaceous species.

3.3. Cell performance

The performance of the single cell, prepared with reference anode material having only Cu as the metal (MCu40/8YSZ/LSM single cell) and using H_2, CH_4 and mixtures H_2/CH_4 as fuels, was discussed in a previous work [9]. The main characterisation results are included in Table 1, single cell (*1*) together with those for single cell with bimetallic anode MCuCo40/8YSZ/LSM, single cell (*2*), for their comparison.

Following the same methodology for preparation and evaluation MCuCo40/8YSZ/LSM single cell (*2*) was prepared. This new single cell was operating at 750 °C for 1450 h under H_2 and/or CH_4, with a total of 1402 h under current demand conditions. During this period, cell was under methane exposure for 39 h. Stable performance was observed during total process. Current demand was fixed to operate the cell under maximum power density condition. The global cell performance as function of current demand and fuel composition is shown in Fig. 5. Methane exposure sequences in the anodic feeding are shown as green solid bars (80:20 CH_4/H_2) and grey bars (100% CH_4).

Prior to fuel-cell testing and after achieving the operation temperature of 750 °C, MCuCo40/8YSZ/LSM single cell (*2*) was polarised in humidified hydrogen (3% H_2O, gas flow = 25 ml min^{-1}), for several hours (70 h) at 105 mA cm^{-2} in order to activate the electrodes. During this period voltage increased from 453 mV to 731 mV (Fig. 5, runtime between 20 and 90 h). Voltage and power versus current (*I–V* and *I–P*) curves for electrode activation process are presented in Fig. 6. Maximum power density undergoes a significant increase from 31 mW cm^{-2} to 88 mW cm^{-2} (Fig. 6a and b) with the electrode activation in humidified hydrogen. After that, anode gas flow (H_2 + 3% H_2O) was adjusted to achieve the highest cell performance, varying between 25 to 60 ml min^{-1}. It was fixed at 50 ml min^{-1} for the study, maximum power density 93 mW cm^{-2} (Fig. 6d), since higher gas flow does not entail significant improvement of cell performance.

After electrode activation, gas flow adjustment and evaluation of single cell (*2*) in humidified hydrogen (maximum power density = 93 mW cm^{-2}), methane was included in the anode feed. A CH_4/H_2 (80:20) mixture and pure methane were used as fuels. The anode had initially been exposed to CH_4/H_2 (80:20) for 1 h and the cell exhibited a power density of only 52 mW cm^{-2}. After operating the cell in CH_4/H_2 mixture, the feed was switched to H_2

Table 1
Main characterisation results for evaluated single cells: (*1*) MCu40/8YSZ/LSM; (*2*) MCuCo40/8YSZ/LSM.

Single cell	Anode	Fuel composition	Cell resistances ($\Omega\,cm^2$)			I_{max} ($mA\,cm^{-2}$)	P_{max} ($mW\,cm^{-2}$)
			R_t	R_p	R_o		
(*1*)	MCu40 [9]	H_2	3.81	2.11	1.70	234	64
		CH_4/H_2 80:20	4.68	2.83	1.85	161	45
(*2*)	MCuCo40	H_2	2.79	1.70	1.09	361	103
		CH_4/H_2 80:20	3.72	2.54	1.18	188	67

Active area: 0.39 cm^2. Electrolyte thickness (mm): 0.25 (*1*), 0.23 (*2*).
Total cell resistance (R_t); ohmic resistance (R_o); polarisation resistance (R_p).

and the power density increased to 97 $mW\,cm^{-2}$, slightly higher value than that observed prior to exposing the anode to methane, remaining stable until the following change in the fuel composition (more than 12 h). Considering this enhancement of cell performance after methane exposure MCuCo40/8YSZ/LSM single cell (*2*) was subjected to three consecutive methane exposure (CH_4/H_2 80:20) cycles, during longer time periods, 1 h, 4 h and 3 h for 2nd to 4th cycle, respectively followed by hydrogen feeding. *I–V* and *I–P* curves were recorded before and after changes in the fuel composition. Fig. 7 comparatively shows the cell voltage and power density as a function of current density and fuel composition, the curves will be denoted hereafter as cycle number-H and cycle number-C depending on whether the fuel is H_2 or CH_4/H_2 (80:20), respectively.

In general, the performance curves and maximum power density when hydrogen was partially replaced for methane (80% v/v) entailed a significant decrease, see Fig. 7 (1st-C to 4th-C plots). The poorer performance for methane compared with H_2 probably results from catalytic limitations [14]. As it has been mentioned above, after the first methane exposure maximum current density operating with hydrogen increased from 93 $mW\,cm^{-2}$ (Fig. 7, 1st-H) to 97 $mW\,cm^{-2}$ (Fig. 7, 2nd-H). Furthermore, single cell performance gradually improved after each cycle (Fig. 7); maximum power densities of 67 $mW\,cm^{-2}$ and 103 $mW\,cm^{-2}$ as well as maximum current densities (cell voltage = 0 V) of 188 $mA\,cm^{-2}$ and 361 $mA\,cm^{-2}$ were achieved running with CH_4/H_2 (80:20) mixture and hydrogen, respectively. This improvement of single cell performance after consecutive cycles of methane exposure may be associated with the formation of carbonaceous deposits on the anode surface providing additional electrical conductivity during the chemical process. It seems that carbonaceous deposits are formed in low level, enough for enhancing the current collection ability of the anode but not promoting the catalytic deactivation on the basis of long-lasting performance of the single cell.

The OCV for single cell operating with humidified hydrogen ($P_{H_2O} = 0.03$ atm) was 1.07 V, this value is consistent with those reported for YSZ-based cells operating on H_2 at this temperature [14]. However, the OCV for CH_4/H_2 (80:20) was 1.0 V, relatively lower than the values that would be predicted from the Nernst equation for complete methane oxidation at this temperature [15]. It is well known that information on anode reaction can be obtained from OCV measurements but, unfortunately, the OCV interpretation under methane is always more complicated because the likelihood of alternative routes for methane oxidation [15,16]. Possible mechanism for the oxidation of methane in humidified atmospheres can be steam reforming (1), direct oxidation (2) or partial oxidation (3); once carbon dioxide, carbon monoxide, hydrogen and steam have been produced then further reactions (4) and (5) can occur in addition to gas shift (6) and cracking (7) and (8):

$$CH_4 + H_2O \rightarrow CO + 3H_2 \quad (1)$$

$$CH_4 + 4O^{2-} \rightarrow CO_2 + 2H_2O + 8e^- \quad (2)$$

$$CH_4 + (1/2)O_2 \rightarrow CO + 2H_2 \quad (3)$$

$$H_2 + O^{2-} \rightarrow H_2O + 2e^- \quad (4)$$

$$CO + O^{2-} \rightarrow CO_2 + 2e^- \quad (5)$$

$$CO + H_2O \rightarrow CO_2 + H_2 \quad (6)$$

$$CH_4 \rightarrow C + 2H_2 \quad (7)$$

$$2CO \rightarrow C + CO_2 \quad (8)$$

Direct methane oxidation (reaction (2)) is theoretically possible using Cu-ceria based anodes [5] but, as pointed out by Marina and Mogensen [17] this reaction is unlikely to take place in one step;

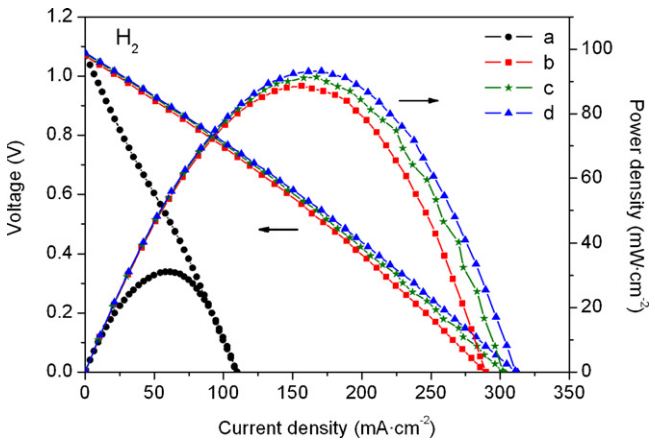

Fig. 6. *I–V* and *I–P* curves of the fuel cell fuelled by humidified hydrogen. (a) Before electrode activation and (b) after electrode activation. Anodic gas flow = 25 ml min^{-1} (b); 40 ml min^{-1} (c); 50 ml min^{-1} (d).

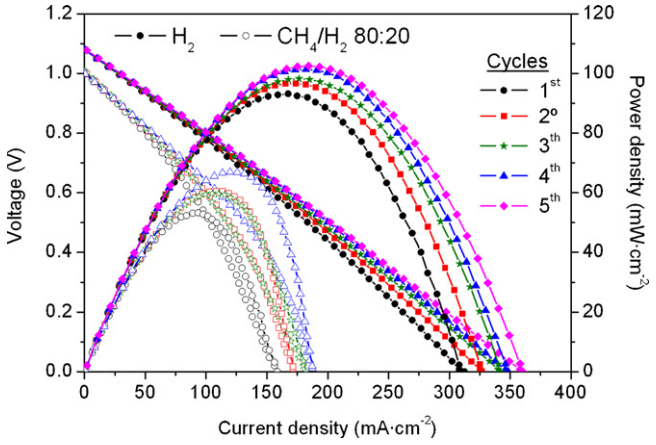

Fig. 7. *I–V* (solid) and *I–P* (hollow) curves of the fuel cell fuelled by hydrogen and H_2/CH_4 mixtures (4 cycles). Methane exposure time for different cycles: 1st cycle (1 h), 2nd (1 h), 3rd (4 h), 4th (3 h).

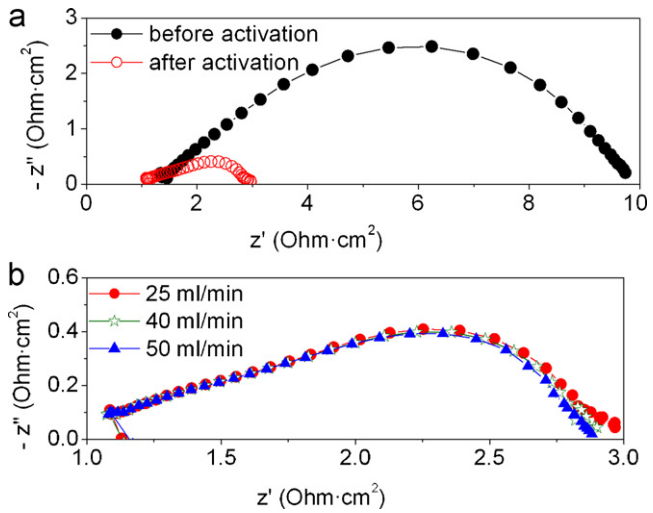

Fig. 8. Impedance spectra for MCuCo40/8YSZ/LSM single cell under humidified hydrogen (3% H_2O) for electrode activation and gas flow variation.

several possibilities exist and the partial oxidation is one of them. Notice that, this study has been carried out using as fuel a mixture of methane/hydrogen (80:20) so an important contribution of reaction (4) is expected. As it has been mentioned above (Section 3.2) the preliminary catalytic activity test for methane oxidation using MCuCo40 as catalyst revealed that CO and H_2 were the majority reaction products of the process. Likewise, CO_2 and H_2O were fairly detected in low concentration. The presence of all these products was corroborated by the GC analysis of the effluent of the anode, with single cell (*2*) running with CH_4/H_2 (80:20) mixture. Taking into account all these consideration, we suggest that the low OCV for CH_4/H_2 mixture results from the establishment of partial oxidation products that remains on anode surface, or nonelectrochemical surface reactions.

The variation of the cell performance was explored in more detail using electrochemical impedance spectroscopy. Figs. 8 and 9 show the impedance spectra measured at open circuit voltage in humidified hydrogen and CH_4/H_2 (80:20) mixtures associated with the IV-curves in Figs. 6 and 7. In these spectra, the intercepts with the real axis at low frequencies represent the total cell resistance (R_t) and the value of the intercept at high frequency is the ohmic resistance (R_o) which includes ionic resistance of electrolyte, electronic resistance of the electrode ands some contact resistances associated with interfaces [18]. The width of the impedance arc on the real-axis is the interfacial polarisation resistance (R_p) that corresponds to the sum of the resistance of the two interfaces: the cathode–electrolyte interface and the anode–electrolyte interface. Fig. 8 shows substantial changes in the resistance values during activation process in humidified hydrogen under constant current demand. Total cell resistance was reduced from 9.88 Ω cm² to 2.97 Ω cm², notice that the highest decrease (70%) corresponding to the polarisation resistance due to the successful electrode activation, whereas, ohmic resistance is reduced <0.3 Ω cm² (Fig. 8a). No significant variation was observed in the cell resistance values when different gas flows were tested (Fig. 8b).

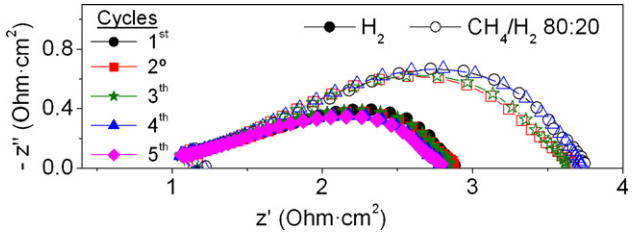

Fig. 9. Impedance spectra for MCuCo40/8YSZ/LSM single cell under humidified hydrogen (3% H_2O) (solid) and CH_4/H_2 (80:20) (hollow).

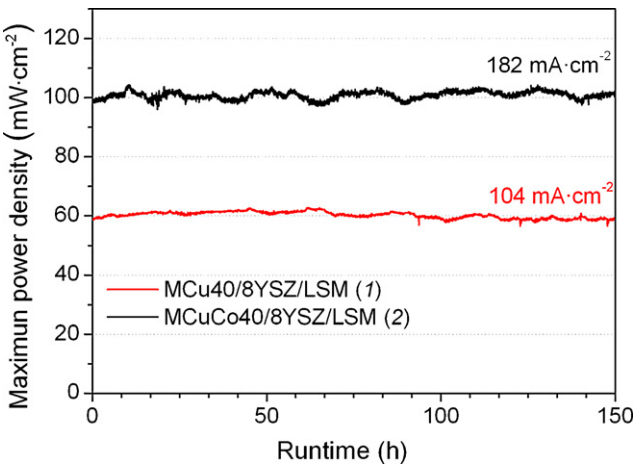

Fig. 10. The maximum power density of the single cells MCu40/8YSZ/LSM (*1*) and MCuCo40/8YSZ/LSM (*2*) as a function of runtime, under humidified hydrogen.

Fig. 9 shows the impedance spectra for hydrogen and methane exposure cycles. It can be observed that cell resistance remains practically constant after them given evidence of no deterioration of the single cell with fuel composition changes. The shapes of impedances spectra are similar running with both fuel compositions. The values of cell resistances were similar for each cycle and composition, minimum differences are observed between cycles, and returns completely to its initial level when methane/hydrogen mixture is switched back to humidified H_2. As expected, the total cell resistance increases with increasing the CH_4 content in the fuel composition affecting in both ohmic resistance and interface polarisation resistance.

The comparison of the main results obtained for single cell evaluation (Table 1) allows to conclude the following statements. For both cells, maximum power densities have been achieved running with humidified hydrogen. In general, the partial substitution of hydrogen for methane in the fuel composition increases the total cell resistance to almost 0.9 Ω cm². When operating on CH_4:H_2 (80:20), the R_o enhances almost 8% for both single cells (*1*) and (*2*) while the increase of R_p was significantly higher, around 26 and 31%, respectively. This increase cannot be due to sintering of metal because the high-frequency intercept returned to its original value when H_2 was reintroduced to the cells (Fig. 9). It might be due

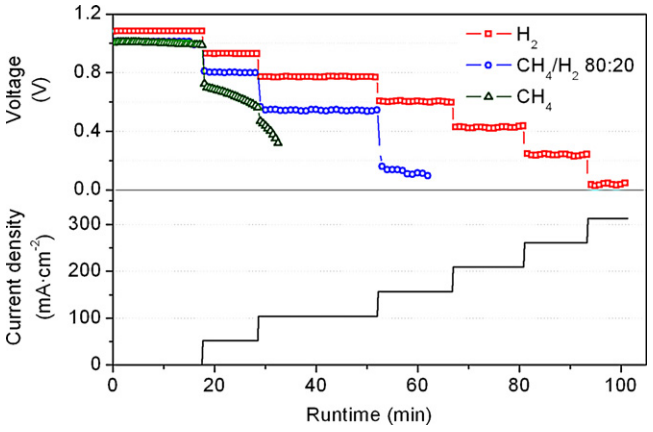

Fig. 11. Cell voltage versus time for MCuCo40/8YSZ/LSM single cell (*2*) as a function current demand and changes in the fuel composition.

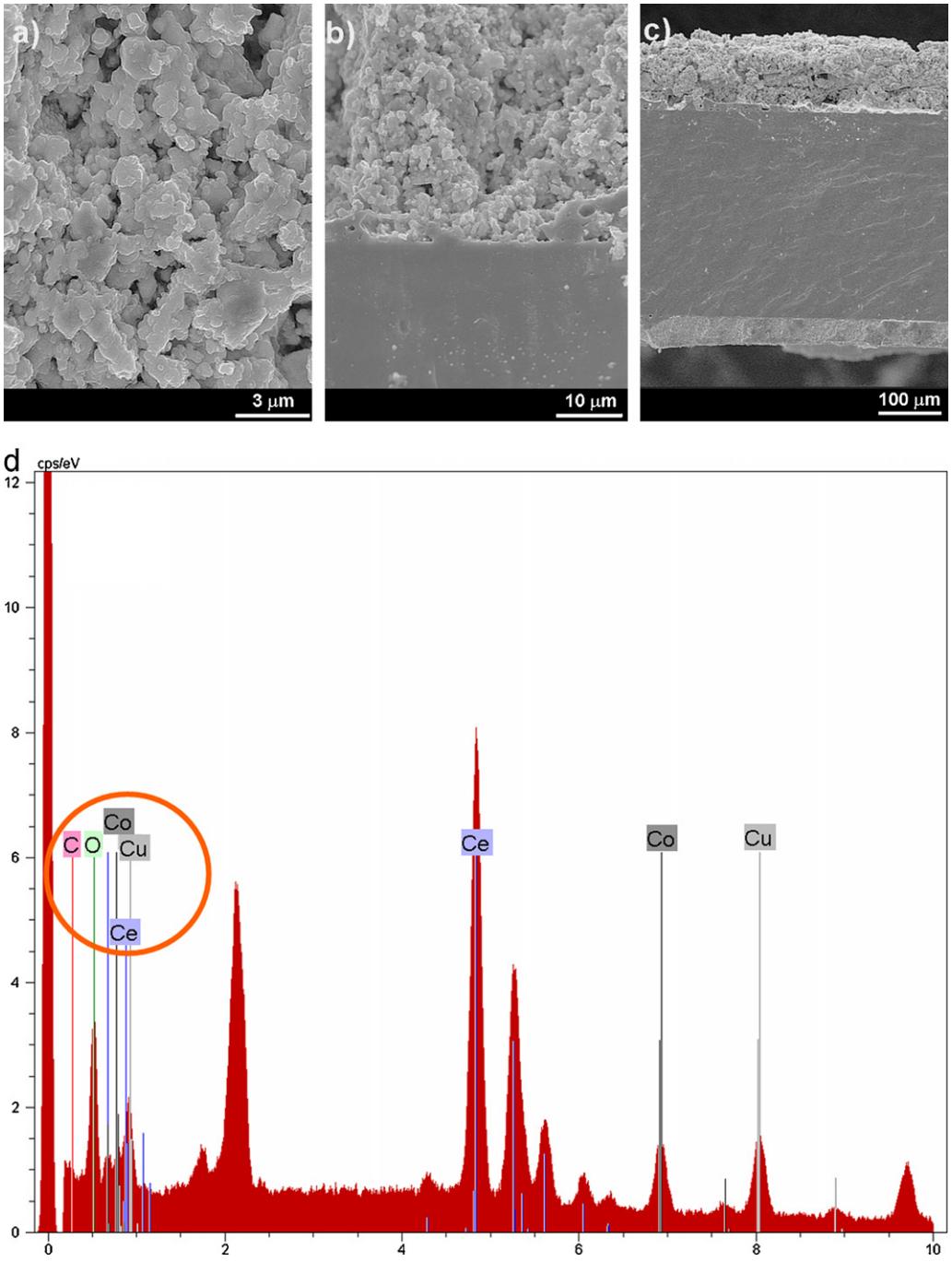

Fig. 12. SEM micrographs of a cross-section of the tested single cell. (a) Anode; (b) anode/electrolyte; (c) anode/electrolyte/cathode and (d) EDX of anode section.

to the lower pO_2 in the anode when running with H_2 compared to hydrocarbon fuel; because the anode contained large amounts of ceria which can provide electronic conductivity when reduced, we suggest that ceria within the anode may be less reduced in the presence of methane.

The partial substitution (20 at.%) of copper by cobalt in the anode composition significantly improves the single cell performance running with different fuels (Table 1). Maximum power densities (P_{max}) undergoes a 38 and 33% increases running in H_2 and CH_4/H_2 80:20, respectively. These results are in good concordance with catalytic activity results that demonstrated higher activity for methane oxidation of MCuCo40 in comparison with MCu40 anode. Independently of fuel, ohmic resistances are lower for single cell (*2*) with smaller electrolyte thickness. Besides, polarisation resistance are reduced with incorporation of cobalt to anode composition, this is ascribed to a favoured charge transfer that increases the efficiency of the triple phase boundary (TPB) process [19].

Fig. 10 shows the result from 150 h test of the both cells (*1*) and (*2*) operating in humidified hydrogen (3% H_2O) under current demand. The maximum power density did not change apparently with runtime, indicating that the anodes are quite stable and have no significant anode deterioration. This result is supported by the SEM data (see Fig. 12). Note that these tests were performed after testing the cell in different fuel environments for 100 h and 350 h for single cell (*1*) and (*2*), respectively, all of which had no effect on the cell performance. Anode including cobalt in its composition allows to achieve a maximum power density of 100 mW cm^{-2} at a

current density of 182 mA cm^{-2} for single cell (*2*), nearly twice than that achieved with Cu-only cell, single cell (*1*).

The operation of both single cells running exclusively with pure methane as fuel was not able; a rapid and constant decrease of cell power was observed. Fig. 11 comparatively shows the cell voltage for MCuCo40/8YSZ/LSM single cell (*2*) at different current demand versus time in hydrogen, CH_4/H_2 80:20 mixture and methane. As shown in Fig. 11, single cell operation under humidified hydrogen was stable with time and current demand. The stability in CH_4/H_2 (80:20) mixture was excellent as long as a cell current density was maintained below 50 mA cm^{-2}. It was only at current density of 60 mA cm^{-2} that voltage decreased gradually over time. Thus, the critical current density to ensure a lasting cell performance was between 0 and 50 mA cm^{-2}, at this temperature and fuel composition. More critical was the result for single cell running with pure methane. At open circuit, the cell voltage slightly decreased over time but when different current demands were applied it decayed significantly. An analysis of *I–V* curves for single cell operation in methane (data not shown) revealed a lost of linearity at higher current, increasing the slope, that suggests an increased electrode concentration polarisation. This phenomenon can be also detected when single cell operates on CH_4/H_2 (80:20) mixture (Fig. 7, -C plots), although to a lower extent.

3.4. Structural single cell characterisation

Fig. 12 illustrates the cross-sectional SEM micrographs of the MCuCo40/8YSZ/LSM (*2*) after single cell evaluation. They were obtained by fracturing the cell, setting it in resin and polishing the exposed cross-sectional surface.

The 8YSZ electrolyte film was essentially dense, with a continuous and crack free surface morphology and no pinholes. Electrodes are well-adhered to the electrolyte and present high interfacial connectivity. Anode exhibits a homogeneous porous microstructure that remains unaltered after operation with hydrogen and methane.

For determining the components of the anode section EDX analysis was performed (Fig. 12d). The presence of characteristic K_α peak of carbon at 0.28 keV gives evidence of the formation of carbon deposits on the anode surface after cell operation. It should be noted that the presence of cobalt (utilisation of MCuCo40 anode) reduce the carbon deposition in comparison with Cu-ceria anode (MCu40) based on the catalytic activity measurements carried out.

4. Conclusions

Anode based on Cu–Co bimetallic doped ceria exhibits good stability for running at relative low temperature (750 °C) under hydrogen and hydrocarbon fuels. The comparison of performance results for two similar single cells, based on 8YSZ electrolyte, LSM cathode and including bimetallic Cu–Co or monometallic Cu-doped ceria as anode revealed that the substitution of 20 at.% of copper for cobalt in the anode composition allows to achieve higher stability against carbon formation with utilisation of methane as fuel and improved performance compared to Cu-only cell. Bimetallic Cu–Co anode showed higher catalytic activity for methane oxidation and favoured charge transfer on the triple phase boundary (TPB).

Note that the ohmic resistances (R_o) are responsible for 45–40% of total cell resistance running with both hydrogen and methane/hydrogen (80:20) respectively. This result suggests that a reduction in the electrolyte thickness together with the use of ceria-based electrolytes, with higher ionic conductivity at this relative low temperature, would produce a significant increase in the overall cell performance.

Acknowledgement

Thanks are due to the Comunidad de Madrid (program DIVERCEL-CM, S2009/ENE-1475) for financial support.

References

[1] A. Atkinson, S. Barnett, R.J. Gorte, J.T.S. Irvine, A.J. McEvoy, M.B. Mogensen, S. Shingal, J.M. Vohs, Nat. Mater. 3 (2004) 17–27.
[2] E.P. Murray, T. Tsai, S.A. Barnett, Nature 400 (1999) 649–651.
[3] S. Park, J.M. Vohs, R.J. Gorte, Nature 404 (2000) 265–267.
[4] J.T.S. Irvine, A. Sauvet, Fuel Cells 1 (2001) 205–210.
[5] S. McIntosh, R.J. Gorte, Chem. Rev. 104 (2004) 4845–4865.
[6] A. Fuerte, A. Hornés, P. Bera, A. Martínez-Arias, M.J. Escudero, L. Daza, ECS Trans. 25 (2009) 2183–2192.
[7] A. Hornés, D. Gamarra, G. Munuera, J.C. Conesa, A. Martínez-Arias, J. Power Sources 169 (2007) 9–16.
[8] S. Lee, J.M. Vohs, R.J. Gorte, J. Electrochem. Soc. 151 (2004) A1319–A1323.
[9] A. Fuerte, R.X. Valenzuela, M.J. Escudero, L. Daza, ECS Trans. 25 (2009) 2173–2182.
[10] A. Fuerte, R.X. Valenzuela, L. Daza, J. Power Sources 169 (2007) 47–52.
[11] N.N. Greenwood, A. Earnshaw, Chemistry of the Elements, Butterworth-Heinemann, Amsterdam, 1997, pp. 1113–1143.
[12] F. Riza, C. Ftikos, F. Tietz, W. Fischer, J. Eur. Ceram. Soc. 21 (2001) 1769–1773.
[13] S. Wang, G.Q. Lu, Ind. Eng. Chem. Res. 36 (1999) 2615–2625.
[14] R.J. Gorte, S. Park, J.M. Vohs, C. Wang, Adv. Mater. 12 (2000) 1465–1469.
[15] K. Kendall, C.M. Finnerty, G. Saunders, J.T. Chung, J. Power Sources 106 (2002) 323–327.
[16] J. Liu, S.A. Barnett, Solid State Ionics 158 (2003) 11–14.
[17] O.A. Marina, M. Mogensen, Appl. Catal. A 189 (1999) 117–126.
[18] K. Yoon, W. Huang, G. Ye, S. Gopalan, U. Pal, D.A. Seccombe, J. Electrochem. Soc. 154 (2007) B389–B395.
[19] D. Pérez-Coll, D. Marrero-López, P. Núñez, S. Piñol, J.R. Frade, Electrochim. Acta 51 (2006) 6463–6469.